Formation of Air Bubbles at Orifices Submerged Beneath Liquids

S. L. SULLIVAN, JR., B. W. HARDY, and C. D. HOLLAND

Texas A&M University, College Station, Texas

The results of two investigations are reported. Air bubbles were formed at orifices submerged beneath each of fourteen liquids. The surface tension of the liquids varied from 17.8 to 72.4 dynes/cm., and the viscosities ranged from 0.436 to 713 centipoise. In the first investigation, air bubbles were formed at orifices at various angles of inclination. Orifice diameters ranging from 0.159 to 0.396 cm. were employed. The air-flow rate was varied from 0.1 to 100 cc. (at standard conditions)/sec. The results were obtained with two different apparatuses by three independent investigators.

In the second investigation, the effect of the velocity of a liquid flowing past a horizontal, submerged orifice on the formation of air bubbles was determined. Liquid velocities ranging from 0.34 to 2.5 cm/sec., which spanned the region of laminar flow, were employed. Orifice diameters ranged from 0.15875 to 0.3175 cm., air-flow rates from 0.5 to 100 cc/sec. (at standard conditions).

It was found that the bubble formation observed in each of these investigations could be correlated with the physical variables of the system by the application of Newton's second law of motion to the bubble at the instant just prior to its release from the orifice.

Several chemical processes depend upon contacting a liquid as a continuous phase with a gas as a dispersed phase. The bubbling of a gas in some manner through a liquid is common to these processes. Geddes (3) attempted to calculate the plate efficiency of distillation columns from the size and number of bubbles contacting the liquid on the distillation trays. This article initiated research on the mechanics of bubble formation. Studies have been made by many investigators of the formation of gas bubbles at horizontal orifices and capillary tubes. However, the early workers neglected the effect of the volume of the chamber upstream from the orifice or capillary tube. Hughes et al. (7), Davidson and Amick (2), and Hayes et al. (6) have demonstrated the importance of the chamber volume. At large chamber volumes, the bubbles form at essentially constant pressure, which is usually the region of interest in industrial applications. All investigators observed two regions of formation, constant-volume and constant-frequency. In the constant-volume region, the volume of the bubble is nearly constant and almost independent of the flow rate of the gas. As the flow rate of the gas was increased, the frequency tended to approach a constant. In the constant-frequency region, the volume of the bubbles was proportional to the gas-flow rate.

Davidson and Amick (2) have described the different regions of bubble formation for horizontal orifices. The formation observed by the authors was essentially the same as that described by Davidson and Amick (2). When the orifice was in the horizontal position, the shape of the bubbles was spherical at low flow rates, and at higher flow rates the bubble became elongated in the direction perpendicular to the orifice. At other angles, the bubbles were spherical at low flow rates and gradually assumed a hemispherical shape as the flow rate was increased. Directly across from the orifice there was a protrusion in the bubble which became more pronounced as the flow rate was further increased.

Hayes et al. (6) showed that the transition from the constant-volume to the constant-frequency region occurs when the force due to the momentum of the gas is equal to the surface-tension force.

In addition to the variation of the type of liquid, the orifice diameter, and the air-flow rates, Sullivan (11) also varied the angle of inclination of the orifice with respect to the horizontal. These data are on file* as well as those data collected by Hayes (5).* Although the effect of the angle on bubble formation is small, it is observable as shown in Figure 1. In spite of the fact that the set of curves for each orifice diameter was reproducible, the ordering of the curves within a set with respect to the orifice angle depended upon the particular diameter of the orifice.

In a second investigation, Hardy (4) determined the effect of the velocity at which a fluid flows past a horizontal orifice (that was submerged in a liquid) on the for-

S. L. Sullivan, Jr., is at Tulane University, New Orleans, Louisiana. B. W. Hardy is with the E. I. du Pont de Nemours and Company, Incorporated, Chattanooga, Tennessee.

* Tabular material has been deposited as document 8093 with the American Documentation Institute, Photoduplication Service, Library of Congress, Washington 25, D. C., and may be obtained for $13.75 for photoprints or $4.50 for 35-mm. microfilm. The data collected by Hayes (5) has been deposited as document No. 5969 with the American Documentation Institute, Photoduplication Service, Library of Congress, Washington 25, D. C., and may be obtained for $3.75 for photoprints or $2.00 for 35-mm. microfilm.

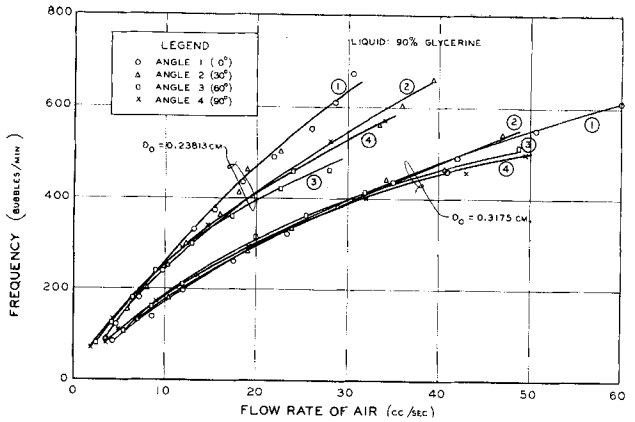

Fig. 1. Effect of the angle of inclination on the frequency of bubble formation.

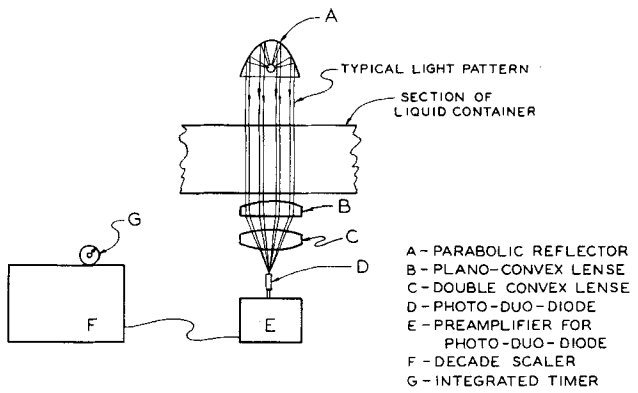

Fig. 3. Sketch of the apparatus used to measure the frequency of bubble formation.

mation of air bubbles at the orifice. A variety of liquids, liquid velocities, orifice diameters, and air rates were used in the investigation. These data are on file.

Qualitatively, the formation of bubbles in a moving liquid stream was essentially the same as that described for horizontal and inclined orifices in fluids at rest. The effect of the velocity of the liquid on the frequency of bubble formation is demonstrated in Figure 2. At low air-flow rates, it is seen that the velocity of the liquid had little effect on the frequency of bubble formation. At the higher gas-flow rates, it was observed in all experiments that at any given air-flow rate, the frequency of bubble formation decreased as the velocity of the liquid was increased.

The physical properties of the liquid phase were varied over wide ranges in the investigations by use of the following liquids: water, glycerine, mixtures of glycerine and water, *n*-propanol, isopropanol, mixtures of isopropanol and water, isooctane, and kerosene.

EXPERIMENTAL

Most of the equipment employed was similar to that used by other experimentors among whom were Hayes et al. (*6*). Thus, only the major variations of the equipment from that commonly employed are described. Detail descriptions are on file* and in references *4* and *11*.

Description of the Equipment Used to Determine the Effect of the Orifice Angle on Bubble Formation

The orifices were holes of known diameter which had been drilled in circular, stainless steel plates. The orifice plates were placed over the end of the orifice holder. The orifice holder [shown by Hayes et al. (*6*)] consisted of a section of 2-in. stainless steel tubing 56 cm. in length.

The liquid container (30 × 25 × 27 in.) in which the orifice holder was mounted was fitted with Plexiglas windows for visual observation of the interior. In order to minimize wall effects, the orifice was placed at least 9 in. from any wall. During the course of the investigation, the orifice plates were located at four different angles with respect to the horizontal, 0, 30, 60, and 90 deg. By the choice of solutions stated above, the physical properties of the liquids were varied over wide ranges.

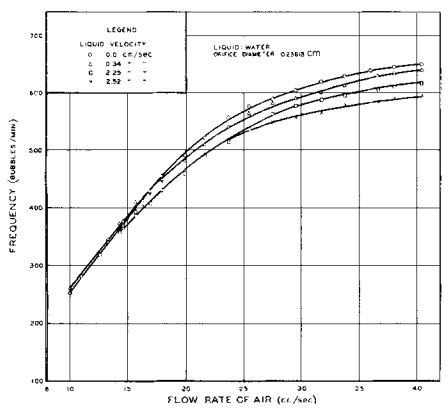

Fig. 2. Effect of the liquid velocity on the frequency of bubble formation.

The frequency of bubble formation was obtained by counting (visually) at low flow rates, and at relatively high flow rates by means of a Strobotac. A method superior to this one was developed by Hardy (*4*) as described in the next section.

Equipment Used to Determine the Effect of Liquid Velocity on Bubble Formation

The orifice holder was inserted in the bottom of the liquid container such that it projected 3 in. into the liquid.

The liquid container was constructed from sheet metal (22 gauge) that was formed into a U shaped channel, which was 67 in. long, 8 in. wide, and 13 in. deep. A sharp-edged weir (9 in. high and 8 in. wide) was attached to the outlet of the liquid container. Thus, the orifice was always submerged beneath at least 6 in. of liquid. At this depth, the formation of bubbles is independent of the depth of submergence (*2, 7*). The orifice holder was located 38.5 in. upstream from the weir. Two windows made of Plexiglas were placed in the sides of the container opposite the orifice holder. The liquid flowed by gravity through the channel, was collected in a tank at the outlet, and recirculated by means of a pump.

A sketch of the photoelectric equipment used to count the number of bubbles formed during a given period of time appears in Figure 3. A 1,000 w. projection bulb contained in a parabolic reflector was used as the light source. The beam of light was passed through a slit which reduced the thickness of the light beam to ¼ in. The slit was located so that the beam of light passed ½ in. above the orifice. Two converging lenses (a plano-convex and a duo-convex) were located on the side of the liquid container opposite the light source. These lenses were used to focus the light rays onto a photo-duo-diode. This photocell was connected to a preamplification circuit, which amplified the change in the output signal of the phototube when a bubble broke the beam of light.

The output from the preamplification circuit was fed to a decade scaler. This particular scaler has a preamplification circuit for the purpose of amplifying signals received from a radiation counter. The output from this preamplification circuit is approximately 10 v. Since the signal from the photocell was also about 10 v., the preamplification circuit of the scaler was eliminated, and the output signal from the photocell was fed directly to the grid circuit of the Schmitt-Trigger circuit of the scaler.

The period of time during which bubbles were counted was controlled by an electric timer which was inserted in the electrical circuit of the decade scaler.

The total rate of flow of liquid through the channel was measured by means of either one or a combination of rotameters, which had been calibrated. The velocity of the liquid past the orifice was determined by measuring the time required for

* See footnote on p. 848.

a hydrometer to flow through a measured length of the channel. A hydrometer was selected such that the bulk of this instrument passed through approximately the same position as that occupied by a bubble during its formation. A plot of the velocity with which the liquid passed by the orifice vs. the volumetric flow rate is shown in Figure 4. For purposes of comparison, the overage velocity is also shown. All of these velocities were within the region of laminar flow (*1*).

DEVELOPMENT OF EQUATIONS

The formation of bubbles at submerged orifices may be described by application of Newton's second law of motion at the instant just prior to the release of the bubble from the orifice. It was possible to correlate all of the data by use of the equations developed for the case where a liquid of velocity $\hat{u}$ flows past an orifice in the horizontal position.

The formation of bubbles in a flowing liquid may be represented by a three-step process as shown in Figure 5. The first two steps are the same as those used by Hayes et al. (*6*) to describe the formation of a bubble at a horizontal orifice beneath a liquid at rest. Superimposed upon the model of Hayes is the velocity $\hat{u}$; that is each point on the surface of the bubble has its horizontal component of velocity increased by $\hat{u}$.

The effect of the angle of inclination of the orifice on the formation of bubbles at an orifice submerged in a liquid at rest ($\hat{u} = 0$) was small, but observable as shown in Figure 1. The ordering of the curves in Figure 1 was reproducible for any given orifice diameter, but no consistent ordering was observed in going from one diameter to another. In an attempt to account for the effect of the angle of inclination of the orifice, various models were investigated such as the one described by Sullivan (*11*). However, no model was found that gave an appreciably better fit than the one obtained from Figure 5 by setting $\hat{u} = 0$. This amounts to taking the formation of a bubble to be independent of the angle of inclination of the orifice with the horizontal. This independence may be accounted for in part by the fact that the bubbles tended to form at the end of a neck (that protruded from the orifice) in essentially the same way that a bubble is formed at a horizontal orifice. The description of the formation of bubbles at a horizontal orifice in a liquid at rest ($\hat{u} = 0$) follows as a special case of the general expressions that are developed.

In the analysis of bubble formation, the velocity of a point on the surface of a spherical bubble that expands

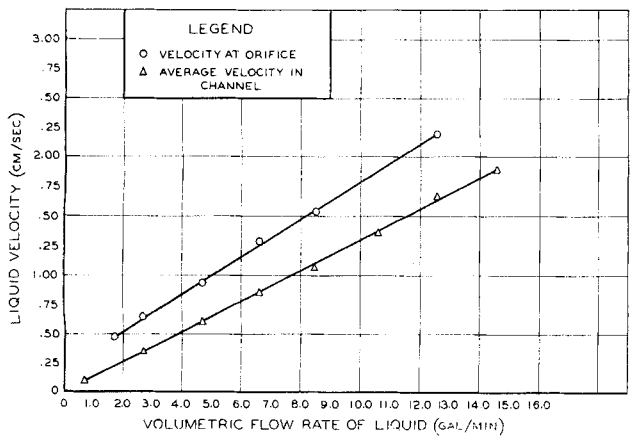

Fig. 4. Variation of the average channel velocity and the velocity at the orifice with the volumetric flow rate.

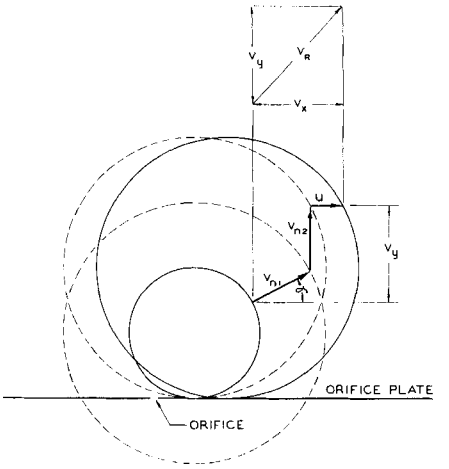

Fig. 5. Velocity of a point on the surface of a bubble during formation.

equally in all directions about a fixed center is needed. For such an expansion

$$\frac{dV}{dt} = q \tag{1}$$

Furthermore

$$\frac{dV}{dt} = \frac{dV}{dD}\frac{dD}{dt} = \pi D^2 \frac{dr}{dt}$$

Let dr/dt be denoted by v_n, the magnitude of the velocity normal to any point on the surface of the sphere. Then

$$v_n = q/\pi D^2 \tag{2}$$

Since the formation of a bubble is a cyclic process, the value of q varies throughout the process of formation of a given bubble. In Equation (2) and in the analysis that follows the instantaneous value of the volumetric flow rate was taken equal to the value that was observed experimentally, which was in effect an average value.

In order to obtain the velocity of a point on the surface of a bubble at any instant during its formation, it is convenient to think of the growth process of a bubble at an orifice as being composed of three steps: first, that the center of a given bubble is fixed and that the bubble experiences an expansion in unit time such that its radius is increased by an amount v_n; second, that each point on the surface of the bubble so formed is displaced vertically by an amount v_n in unit time; and third, that the bubble is displaced horizontally by the flowing liquid a distance u (the speed of the liquid) in unit time. The vector representation of this three-step growth process is shown in Figure 5. Let the velocity vectors of steps 1, 2, and 3 be denoted by $\hat{v}_{n1}$, $\hat{v}_{n2}$, and $\hat{u}$, respectively. Thus the velocity $\hat{v}_R$ of a point on the surface is given by the vector sum

$$\hat{v}_R = \hat{v}_{n1} + \hat{v}_{n2} + \hat{u} \tag{3}$$

It is readily shown that the average of the magnitude of the vertical component of the velocity (denoted by $\bar{v}_y$) of a point on the surface of a bubble is equal to v_n. The magnitude of the vertical component of $\hat{v}_R$ is given by $v_y = \hat{v}_R \cdot \hat{j}$. Since $\hat{u} \cdot \hat{j} = 0$, the expression for v_y reduces to the one obtained by Hayes et al. (*6*) (for the case $\hat{u} = 0$), who showed that

$$\bar{v}_y = v_n \tag{4}$$

where $v_{n1} = v_{n2} = v_n$. Thus, it has been shown that the

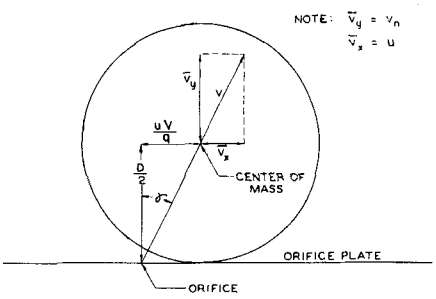

Fig. 6. Movement of the center of mass with respect to the orifice.

average of the vertical component of the velocity over the surface of a bubble is equal to the vertical component of the velocity of its center of mass.

Examination of Figure 6 shows that the center of mass of the bubble moves away from the orifice in the horizontal direction at the average speed u. The magnitude of the horizontal component of $\hat{v}_R$ at any point on the surface is given by $v_x = \hat{v}_R \cdot \hat{i}$. It is readily shown (see reference 4) in a manner analogous to that used by Hayes et al. (6) for the vertical component, that the average of v_x over the surface is given by

$$\bar{v}_x = u \tag{5}$$

Thus, the average of the horizontal and vertical components of velocity over the surface of a bubble are equal to the corresponding components of the center of mass of the bubble.

Forces Acting on a Bubble

The formation of a bubble at a submerged orifice is a variable mass type of problem. Pars (8) has shown that when to a body that is moving with the instantaneous velocity $\hat{v}$ (relative to a fixed observer), mass traveling with the velocity $\hat{v}_o$ (relative to a fixed observer) is added at the rate dm/dt, one must include the force $\hat{v}_o(dm/dt)$ in the application of Newton's second law of motion. Since $\hat{v}_o \cdot \hat{j} = v_o$, the vertical component of this force is $v_o(dm)/(dt)$. For the case where a liquid flows past an orifice with the velocity $\hat{u}$, it is supposed that a short neck having a diameter D_o connects the orifice with the bubble. The neck makes an angle γ with the vertical axis of the orifice, see Figure 6. Other forces acting in the vertical direction are as follows: the net buoyancy force $gV\Delta\rho$ and the excess pressure force $(\pi D_o^2/4)\ (p_i - p)\ \cos\gamma$, the surface tension force $\pi D_o\sigma \sin\gamma$, the drag force F_D, and the force F_I required to overcome the inertia of the fluid surrounding the bubble. When the actual bubble is replaced by one moving with the instantaneously velocity equivalent to the average values $(\bar{v}_x, \bar{v}_y)$ and with the same set of forces acting on its external surface, Newton's second law of motion yields

$$v_o\frac{dm}{dt} + gV\Delta\rho + \frac{\pi D_o^2}{4}(p_i - p)\cos\gamma - \pi D_o\sigma\cos\gamma - F_D - F_I = \frac{d(m\bar{v}_y)}{dt} \tag{6}$$

for the sum of the forces in the vertical direction. When the net buoyancy force is taken to be $gV\Delta\rho$, it is implied that the hydrostatic pressure p instead of the actual pressure p_i acts over the area of the bubble immediately above the orifice. Hughes et al. (7) included the excess pressure force to account for the error in the expression for the net buoyancy. The fact that a pressure slightly greater than p_i is required for the gas to flow from the orifice to various parts of the expanding bubble is neglected in the present treatment. The pressure difference $(p_i - p)$ was approximated by the well-known relationship

$$p_i - p = \frac{4\sigma}{D} \tag{7}$$

Prandtl (9) has given an informative derivation of this relationship.

The drag force accounts for the friction and form drag on the bubble. Since it is assumed that the bubble moves in the horizontal direction at the same velocity $\hat{u}$ as that of the liquid, there is no net flow of liquid around the bubble in the horizontal direction. Drag on the bubble occurs because the bubble passes through the liquid in the vertical direction at the speed $\bar{v}_y = v_n$. The drag force was expressed in terms of the drag coefficient as follows:

$$F_D = \frac{C_D\rho_L(\bar{v}_y)^2(\pi D^2/4)}{2} \tag{8}$$

Consider next the force necessary to overcome the inertia of the liquid. For a bubble moving with the instantaneous velocity $\hat{v}$ through a liquid at rest, this force is given by $m^1(dv/dt)$. Since the model assumes that the bubble moves through the liquid in the vertical direction with the speed $\bar{v}_y$ and with the liquid in the horizontal direction with the speed u, it follows that the force required to overcome the inertia of the liquid is given by

$$F_I = m^1\frac{d\bar{v}_y}{dt} \tag{9}$$

where m^1 is an effective mass of the displaced fluid. For irrotational flow Streeter (10) has shown that m^1 is one-half on the mass of the displaced fluid. In the treatment by Hayes et al. (6), m^1 was assumed to be proportional to the mass of the displaced liquid. Thus

$$m^1 = \chi V\rho_L \tag{10}$$

For irrotational motion the quantity χ is of course equal to ½, but since it was not irrotational, the quantity χ and the drag coefficient were correlated as a power function of the appropriate dimensionless groups as shown in a subsequent section.

When the forces are summed in the horizontal direction, Newton's second law of motion gives

$$\frac{\pi D_o^2}{4}(p_i - p)\sin\gamma - (\pi D_o\sigma)\sin\gamma = \frac{d(m\bar{v}_x)}{dt} \tag{11}$$

Multiplication of Equation (6) by $\cos\gamma$ and Equation (11) by $\sin\gamma$ followed by addition and rearrangement yields

$$gV\Delta\rho - (\pi D_o\sigma\sec\gamma)\ (1 - D_o/D) - \frac{C_D\rho_L\ (\bar{v}_y)^2\ (\pi D^2/4)}{2} - \chi V\rho_L\frac{d\bar{v}_y}{dt} = -v_o\frac{dm}{dt} + \frac{d(m\bar{v}_y)}{dt} + (\tan\gamma)\frac{d(m\bar{v}_x)}{dt} \tag{12}$$

where F_D, F_I, $(p_i - p)$, and m^1 have been replaced by the relationships given by Equations (7) through (10). By use of the relationships given by Equations (1), (2), (4), (5), and those that follow

$$m = V\rho_g;\ \frac{dm}{dt} = \rho_g q;\ \frac{d\bar{v}_y}{dt} = -\frac{4q^2}{\pi^2 D^5};\ \frac{d(m\bar{v}_x)}{dt} = u\rho_g q$$

$$\frac{d(m\bar{v}_y)}{dt} = \frac{q}{3}\rho_g v_n;\ v_o = (4q)/D_o^2\pi;$$

$$N_{Fr} = v_n^2/(Dg) = q^2/(\pi^2 D^5 g) \qquad (13)$$

it is readily shown that Equation (12) may be stated in the following form:

$$Vg\,\Delta\rho(1-\psi) = (\pi D_o \sigma \sec\gamma)\,(1 - D_o/D) - \phi \qquad (14)$$

The quantities ψ and ϕ are defined as follows:

$$\psi = \frac{3\,\rho_L}{4\,\Delta\rho}(N_{Fr})\left[C_D - \frac{16\,\chi}{3}\right] \qquad (15)$$

$$\phi = \frac{4q^2\,\rho_g}{\pi D_o^2}\left[1 - \frac{1}{12}\left(\frac{D_o}{D}\right)^2\right] - u\rho_g q \tan\gamma \qquad (16)$$

From Figure 6, it follows that

$$\gamma = \tan^{-1}\frac{(uV)/q}{D/2} \qquad (17)$$

Both the interpretation of Equation (14) and the use of it to correlate the data are presented in the sections that follow.

INTERPRETATION OF EXPERIMENTAL RESULTS

Development of the Equations for the Constant-Volume and Constant-Frequency Regions

In the interpretation of the experimental results, Equation (14) was applied at the instant just prior to the release of the bubble from the orifice (or neck). The values of the variables at this time were determined experimentally. When one follows Hayes et al. (6), the positive difference $|1 - \psi|$ is correlated as a function of the Froude and Reynolds numbers and the ratio of the diameters as follows:

$$|1-\psi| = k(N_{Re})^a(N_{Fr})^b(D_o/D)^c \qquad (18)$$

a, b, c, and k are constants, and

$$N_{Re} = \frac{Dv_n\,\rho_L}{\mu_L} = \frac{q\,\rho_L}{\mu_L\,\pi D}$$

That ψ is a function of both the Froude and Reynolds numbers is demonstrated by Equation (16), since the drag coefficient is a function of the Reynolds number.

Examination of Equation (14) shows that the left-hand side represents the difference between the net buoyancy and the drag types of forces, and the right-hand side represents the difference between the net surface-tension force and momentum types of forces. When the net surface-tension forces are balanced by ϕ, the right-hand side of Equation (14) is equal to zero. Hence, the left-hand side is also zero, which requires that the net buoyancy and ψ be in balance. The condition where each side of Equation (14) is identically equal to zero was used to divide the data into the constant-volume and constant-frequency regions. Hayes et al. (6) have shown that the break point between the constant-volume and constant-frequency regions may be accurately predicted by solving the following equation for q:

$$(\pi D_o\,\sigma\sec\gamma)\,(1 - D_o/D) = \phi \qquad (19)$$

This break point was used to divide the data into two groups as follows:

Constant-volume region: $(\pi D_o\,\sigma\sec\gamma)\,(1 - D_o/D) > \phi$

Constant-frequency region: $(\pi D_o\,\sigma\sec\gamma)\,(1 - D_o/D) < \phi$

In the constant-volume region, the volume of the bubbles varied little, but the frequency of formation varied considerably with the air-flow rate. In the constant-frequency region, the situation was reversed. In the constant-volume region, the frequency of formation was chosen as the dependent variable. For the runs in the constant-frequency region, the volume of the bubble was chosen as the dependent variable.

Since

$$V = q/f \text{ and } D = (6q/\pi f)^{1/3}$$

the Reynolds and Froude numbers appearing in Equation (18) may be stated in terms of the frequency as follows:

$$\bar{N}_{Re} = \frac{(q^2 f/6\pi^2)^{1/3}\rho_L}{\mu_L} = N_{Re}\,f^{-1/3} = \frac{q^{2/3}\rho_L}{(\pi^2 6^5)^{1/3}\mu_L}$$

$$\bar{N}_{Fr} = \frac{(qf^5/\pi 6^5)^{1/3}}{g} = N_{Fr}\,f^{-5/3} = \frac{q^{1/3}}{(\pi 6^5)^{1/3} g}$$

These equations define the modified Reynolds and Froude numbers, $\bar{N}_{Re}$ and $\bar{N}_{Fr}$, which are independent of the frequency of formation and the bubble volume. Equations (14) and (18) may be solved for either the frequency of bubble formation or the bubble volume in terms of the physical properties of the liquid and gas phases, the flow rate of the gas q, and the angle γ as follows:

$$f = k\bar{N}_{Re}^{-3}\,[Nq\bar{N}_{Re}^{-3}]^a[\bar{N}_{Fr}\bar{N}_{Re}^{-5}]^b\,[D_o(\pi/6q)^{1/3}\,\bar{N}_{Re'}^{-1}]^c \qquad (20)$$

$$V = k(N_{Re'})^{-3}[N^{-1}(N_{Re'})^{-3}]^a[N_{Fr'}(N_{Re'})^{-5}]^b\,[D_o(\pi/6)^{1/3}(N_{Re'})^{-1}]^c \qquad (21)$$

where

$$N = \left|\frac{g\Delta\rho}{(\pi D_o\,\sigma\sec\gamma)\,(1 - D_o/D) - \phi}\right|$$

$$N_{Re'} = N_{Re}\,V^{1/3} = \frac{q\rho_L}{(\pi^2 6)^{1/3}\mu_L}$$

$$N_{Fr'} = N_{Fr}\,V^{5/3} = \frac{q^2}{(\pi 6^5)^{1/3} g}$$

It should be noted that although the same symbols are used to represent constants in Equations (18), (20), and (21), the values of these constants, of course, differ in each of the equations.

The modified Reynolds and Froude numbers that appear in Equations (20) and (21) were employed in order that these equations might be solved explicitly for either f or V as a function of the operating variables and physical properties of the liquid and gas phases. Actually, the bubble diameter D does appear in the number N on the right-hand side of these equations. However, since the terms that involved D varied little over the range of operating conditions, the quantity N was relatively insensitive to bubble diameter. Thus, the use of modified numbers in effect eliminated the correlating of a variable against itself. In the first attempt to correlate the data, they were divided into the constant-volume and constant-frequency regions by use of the criteria given immediately after Equation (19). In the examination of the results so obtained, it was observed that for frequencies less than about 5 bubbles/sec. the calculated values of the frequencies were consistently larger than the experimental values. Because of this, the data for the constant-volume region were subdivided into two groups as implied by the conditions that precede Equations (22) and (23).

On the basis of this division of the data, the constants in Equations (20) and (21) were determined from a non-

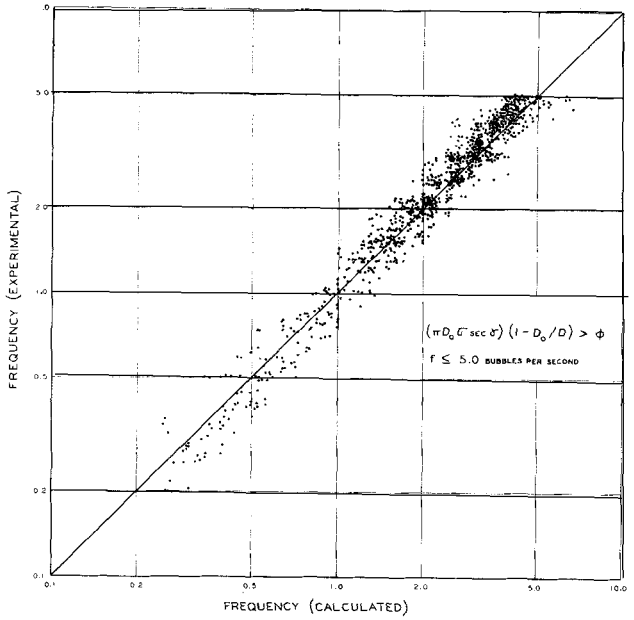

Fig. 7. Comparison of experimental and calculated values of the frequency of bubble formation.

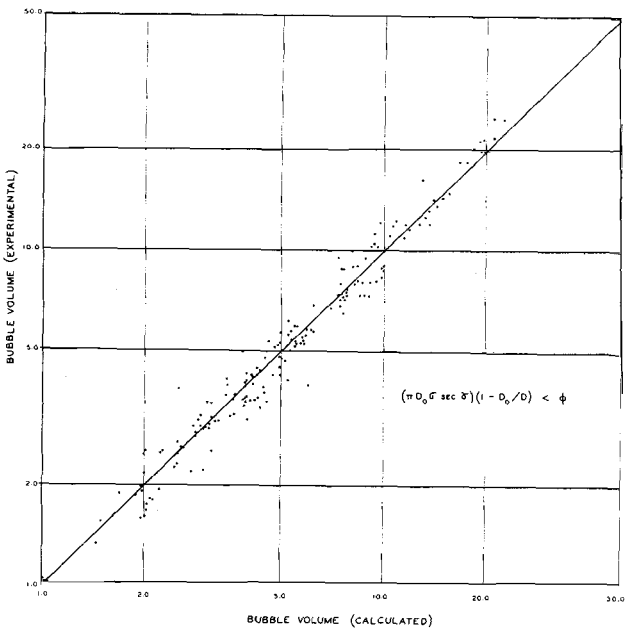

Fig. 9. Comparison of experimental and calculated values of the bubble volume.

linear regression analysis of the experimental data by use of digital computer. The sum of the squares of the fractional deviation (experimental value minus the calculated value, divided by the experimental value) was required to be a minimum. A total of 2,013 observations were used in the regression analysis. Certain of the original data were discarded on the basis of the following reasons. In the case of the multiple formation of bubbles, different conventions for counting the multiple bubbles were employed by Hayes et al. (*6*) and Sullivan (*11*). Also the frequencies of formation as determined by these investigators by use of a Strobatac were relatively inaccurate. Since most of the multiple formation occurred with the smaller orifices, all of the data collected by Hayes et al. and Sullivan with orifices having a diameter of 0.159 cm. or less were discarded. However, all of the data collected by Hardy were used because the accuracy of the photoelectric method was good in the region of multiple bubble formation. The smallest positive value of the denominator of N used in the correlation of the data for the constant-volume region was 1.29, and the smallest negative value of the denominator used in the correlation of the data for the constant-frequency region was 0.83. For values of the denominator lying between these two, the relationship for the breakpoint, Equation (19), is recommended over the correlations that follow.

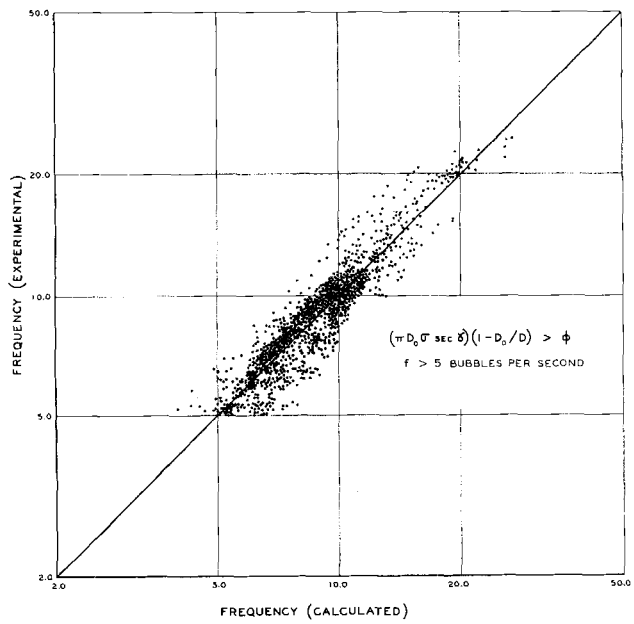

Fig. 8. Comparison of experimental and calculated values of the frequency of bubble formation.

The average deviations for the three regions of bubble formation were 12.5, 10.2, and 11.2%. Three sets of values for k, a, b, and c were obtained. These were used in to restate Equations (20) and (21) in the following convenient computational forms:

For $\pi D_o \sigma \sec \gamma \,(1 - D_o/D) > \phi$ and $f \leqq 5$:

$$\frac{f}{N^{0.456}} = 0.00632\, N_{Re}^{-2.588}\, \overline{N}_{Fr}^{0.175}\, q^{0.758}\, D_o^{-0.905} \qquad (22)$$

For $\pi D_o \sigma \sec \gamma \,(1 - D_o/D) > \phi$ and $f \geqq 5$:

$$\frac{f}{N^{0.147}} = 0.0096\, \overline{N}_{Re}^{-0.785}\, \overline{N}_{Fr}^{-0.286}\, q^{0.654}\, D_o^{-1.226} \qquad (23)$$

For $\pi D_o \sigma \sec \gamma \,(1 - D_o/D) < \phi$:

$$\frac{V}{N^{-0.0188}} = 80.1\, N_{Re'}^{-0.67}\, N_{Fr'}^{0.330}\, D_o^{1.372} \qquad (24)$$

A comparison of the calculated and experimental values of f (or V) is presented in Figures 7, 8, and 9. For the data of Hayes (5) (collected at horizontal orifices in liquids at rest, $\gamma = 0$) the average deviations for the three regions were 15.2, 11.1, and 11.0%. For Sullivan's (*11*) data (collected at various orifice angles in liquids at rest, $\gamma = 0$), the average deviations for the three regions were 12.5, 10.4, and 12.4%. For Hardy's (*4*) data ($\gamma \neq 0$), the average deviations were 10.7, 9.8, and 10.5%.

For any given set of operating conditions, the right-hand sides of Equations (22), (23), and (24) are completely determined. Since N depends on f (or V), the trial-and-error involved in the use of these equations consists of finding a value of f (or V) that satisfies an equation of the form

$$\frac{f}{N^{(0.456 \text{ or } 0.147)}} = \text{constant, or } \frac{V}{N^{-0.0188}} = \text{constant}$$

The amount of trial and error is further reduced by noting that the variation of $(1 - D_o/D)$ with respect to D_o was bounded as follows:

D_o, cm.	$(1 - D_o/D)$, min.	$(1 - D_o/D)$, max
0.15875	0.8538	0.8767
0.23813	0.8214	0.8574
0.3175	0.7951	0.8395

In view of the large number of experimental observations, the number of variables considered, and the use of the results obtained on different apparatuses by different experimenters, it is felt that bubble formation is adequately described (over the range of the variables employed in the experiments) by the correlations given by Equations (22), (23), and (24).

ACKNOWLEDGMENT

This work was supported by the National Science Foundation, and the Engineering Experiment Station of the Texas A&M University. This aid is gratefully acknowledged.

NOTATION

a = constant, dimensionless
A_o = area of the orifice, L^2
b = constant, dimensionless
c = constant, dimensionless
C_D = drag coefficient, dimensionless
D = diameter of the bubble (assumed to have a spherical shape), L
D_o = diameter of the orifice, L
f = frequency of bubble formation, T^{-1}
F_D = drag force, ML/T^2
F_I = force required to overcome the inertia of the liquid, ML/T^2
g = acceleration due to gravity, L/T^2
k = constant, dimensionless
$\hat{i}$ = unit vector in the horizontal direction
$\hat{j}$ = unit vector in the vertical direction
m = mass of the bubble at any time t, M
m^1 = mass term for the displaced fluid, M
N = term defined below Equation (21), L^{-3}
N_{Fr} = Froude number, defined by Equation (13), dimensionless
N_{Re} = Reynolds number, defined below Equation (18), dimensionless
$\overline{N}_{Fr}$ = modified Froude number, defined after Equation (19), $T^{5/3}$
$\overline{N}_{Re}$ = modified Reynolds number, defined after Equation (19), $T^{1/3}$
$N_{Fr'}$ = modified Froude number, defined after Equation (21), $L^{5/3}$
$N_{Re'}$ = modified Reynolds number, defined after Equation (21), $L^{1/3}$
p = hydrostatic pressure at a depth of submergence equal to that of the orifice, M/LT^2
p_i = pressure inside the bubble, M/LT^2
q = volumetric rate of flow of the gas evaluated at the conditions at the top of the orifice (because of the small pressure drops involved, the pressure and temperature were taken equal to those in the orifice holder in the calculation of q), L^3/T
r = radius of the bubble (assumed to have spherical shape), L
t = time, T
$\hat{u}$ = velocity of the liquid at a point about ½ in. above the orifice, L/T
$\hat{v}$ = velocity, L/T
$\hat{v}_n$ = velocity normal to the surface of the bubble, L/T
$\hat{v}_o$ = velocity of the gas through the orifice, L/T
$\hat{v}_R$ = velocity of a point on the surface of the bubble, L/T
v_x = magnitude of the horizontal component of the velocity at any point on the surface of the bubble; $\overline{v_x}$ is the average of v_x over the surface of the bubble, L/T
v_y = magnitude of the vertical component of the velocity at any point on the surface of the bubble; $\overline{v_y}$ is the average of v_y over the surface of the bubble, L/T
$\hat{v}_{n1}, \hat{v}_{n2}$ = velocity vectors, see Figure 5, L/T
V = volume of the bubble at the instant before its release from the orifice, evaluated at the experimental conditions of the gas in the orifice holder, L^3
z = depth of submergence, L

Greek Letters

α = angle used in the vector diagram, see Figure 5, rad.
$\Delta\rho$ = density of the liquid minus the density of the gas, M/L^3
μ_L = viscosity of the liquid, M/LT
π = 3.1416
ρ = density, M/L^3
ρ_g = density of the gas evaluated at the temperature and pressure in the gas chamber, M/L^3
ρ_L = density of the liquid, M/L^3
σ = interfacial tension between the liquid and air, M/T^2
ϕ = variable, defined by Equation (16), ML/T^2
χ = function, defined in Equation (10), dimensionless
ψ = variable, defined by Equation (15), dimensionless
γ = angular measure of the movement of the center of mass in the horizontal direction, see Figure 6

Mathematical Symbol

$|x|$ = absolute value of x

LITERATURE CITED

1. Chow, Ven Te, "Open-Channel Hydraulics," pp. 3-23, McGraw-Hill, New York (1959).
2. Davidson, Leon, and E. H. Amick, Jr., *A.I.Ch.E. Journal*, **2**, 337 (1956).
3. Geddes, R. L., *Trans. Am. Inst. Chem. Engrs.*, **42**, 79 (1946).
4. Hardy, B. W., Dissertation, Texas A&M University, College Station, Texas (1964).
5. Hayes, W. B., III, Dissertation, A. and M. College of Texas, College Station, Texas (May, 1958).
6. ———, B. W. Hardy, and C. D. Holland, *A.I.Ch.E. Journal*, **5**, 319 (1959).
7. Hughes, R. R., A. E. Handlos, H. D. Evans, and R. L. Maycock, *Chem. Eng. Progr.*, **51**, 557 (1955).
8. Pars, L. A., "Introduction to Dynamics," pp. 162-165, Cambridge University Press, Cambridge, England (1953).
9. Prandtl, Ludwig, "Essentials of Fluid Dynamics," Authorized translation, pp. 26-30, Hafner Publishing Co., New York (1952).
10. Streeter, V. L., "Fluid Dynamics," pp. 64-67, McGraw-Hill, New York (1948).
11. Sullivan, S. L., Jr., Dissertation, Texas A&M University, College Station, Texas (1963).

Manuscript received June 11, 1963; revision received April 23, 1964; paper accepted May 6, 1964.